Cation and anion dynamics in supercooled and glassy states of the ionic liquid 1-butyl-3-methylimidazolium hexafluorophosphate: Results from ^{13}C, ^{31}P, and ^{19}F NMR spectroscopy

Takatsugu Endo,[1] Scarlett Widgeon,[2] Ping Yu,[2] Sabyasachi Sen,[2,*] and Keiko Nishikawa[1]

[1]*Graduate School of Advanced Integration Science, Chiba University, 1-33 Yayoi-cho, Inage-ku, Chiba 263-8522, Japan*

[2]*Department of Chemical Engineering and Materials Science, One Shields Avenue, University of California, Davis, California 95616, USA*

(Received 20 December 2011; revised manuscript received 27 January 2012; published 27 February 2012)

The rotational dynamics of cations and anions in the room temperature ionic liquid, 1-butyl-3-methylimidazolium hexafluorophosphate ($[C_4mim]PF_6$) have been investigated in the supercooled liquid and glassy states using ^{13}C, ^{31}P, and ^{19}F NMR spectroscopy. The α-relaxation process of the supercooled liquid corresponds well with that of the isotropic rotational reorientation of the $[C_4mim]^+$ cations. The timescale of the reorientational motion of the butyl chain in the cations, which is reminiscent of the conformational isomerization, is found to be slower than that of the imidazolium ring. This counterintuitive result can be attributed to the presence of local structures in the form of polar and nonpolar nanodomains in the liquid and significant steric and coulombic interactions between the rings or chains in the cations and such domains. On the other hand, the dynamics of the constituent PF_6^- anions is dominated by free rotational diffusion at temperatures above ~230 K, while a restricted rotational or librational motion dominates at lower temperatures. This transition temperature can be identified with the mode coupling critical temperature T_c where the anion rotational timescale decouples from that of the $[C_4mim]^+$ cations. The librational motion of the anions has a characteristic timescale on the order of 10^{-10} s with an activation energy of ~0.16 eV typical of a β-relaxation process. This dynamical process continues below T_g, well into the glassy state of this ionic liquid.

DOI: 10.1103/PhysRevB.85.054307 PACS number(s): 64.70.pm, 78.30.cd, 76.60.−k, 61.20.Lc

I. INTRODUCTION

Room temperature ionic liquids (RTILs) are salts that are liquid at or near room temperature. RTILs are characterized by a number of remarkable physical-chemical properties, such as negligible vapor pressure, extremely low flammability, high thermal stability, and large electrochemical window. These interesting materials have recently attracted much attention because of their potential use as electrolytes in batteries, as green solvents for organic syntheses, and for CO_2 sequestration, to name a few.[1–5] Many RTILs are also known to be good glass formers. Unfortunately there are only a handful of studies in the literature on the glass transition of RTILs in spite of the fact that the phenomenon of glass transition remains one of the most important unsolved problems in contemporary physics.[6–9] The glass transition process of RTILs has been studied primarily using calorimetry[10–16] and dielectric spectroscopy.[17–27] These studies provided some important insights into the glass transition phenomena, however, a clear understanding of the atomic scale mechanisms of ionic motions associated with the viscous slowdown and glass transition remains lacking.

In this work, we have investigated the dynamics of the constituent cations and anions in the RTIL 1-butyl-3-methylimidazolium hexafluorophosphate ($[C_4mim]PF_6$) in the supercooled liquid and glassy state using multinuclear (^{13}C, ^{31}P, ^{19}F), high-resolution and variable temperature nuclear magnetic resonance (NMR) spectroscopy. $[C_4mim]PF_6$ was selected for this study because it is one of the most widely studied materials in relation to the glass transition of RTILs.[11,16,18,19,23,28–34] Analyses of NMR powder pattern line shapes and spin-lattice relaxation times (T_1) provide information on site-specific ionic dynamics over timescales ranging between 10^{-3} s and 10^{-12} s.

II. EXPERIMENT

A. Synthesis

$[C_4mim]PF_6$ was prepared by metathesis of 1-butyl-3-methylimidazolium bromide with sodium hexafluorophosphate. The RTIL was purified by washing with distilled water and by filtering through activated charcoal. The final product was characterized by ^{1}H-NMR (JEOL JNM-LA500) and by elemental analysis (Perkin-Elmer 2400). No bromine ions could be detected on adding aqueous $AgNO_3$ solution to the RTIL. The RTIL was dried under a vacuum of about 10^{-3} Pa at 333 K for one day before use. The sample was handled in a glovebox in N_2 atmosphere to avoid absorption of atmospheric moisture. The water content of the RTILs was ca. 100 ppm, as measured by Karl Fischer titration using a Mettler-Toledo model DL39 coulometer. The structure and abbreviations for all carbons for $[C_4mim]PF_6$ are shown in Fig. 1. The melting point and the glass transition temperature T_g are 284.3 K and 192 K, respectively.[35] Note that as an RTIL the $[C_4mim]PF_6$ is well suited for NMR measurements since all the nuclides in this material are detectable in principal by NMR spectroscopy.

B. NMR spectroscopy

All NMR measurements were carried out under static (nonspinning) conditions with a Bruker 7 mm variable temperature CP-MAS probes and a Bruker Avance 500 solid-state spectrometer operating at resonance frequencies of 125.8, 202.5, and 470.6 MHz for ^{13}C, ^{31}P, and ^{19}F, respectively. Samples were taken in zirconia rotors, and NMR spectra were collected over a temperature range of 292 K to 174 K upon cooling. An isothermal holding period of 3 minutes before data collection was found to be sufficient to ensure thermal

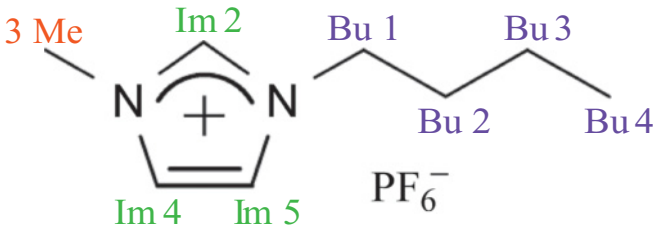

FIG. 1. (Color online) Schematic of the structure of $[C_4mim]PF_6$ molecule and abbreviations used in the text for all carbon sites.

equilibration. The ^{13}C and $^{19}F/^{31}P$ spectra were collected in separate runs to minimize the data collection time at each temperature and thereby to avoid crystallization of the supercooled liquid. At each temperature the acquisition time for the ^{13}C and $^{19}F/^{31}P$ spectra were approximately 15–30 and 10–20 minutes, respectively. ^{13}C NMR spectra above 235 K were measured with a $\pi/2$ pulse (4.5 μs) and high power proton decoupling (HPPD) using two pulse phase modulated (TPPM) proton decoupling[36] with a phase modulation angle of 15° and a ^1H decoupling frequency of 20.8 kHz. Typically a recycle delay of 10 s was used. ^{13}C NMR spectra below 226 K were measured with $^{13}C\leftarrow{}^1H$ cross polarization (CP) and HPPD. These spectra were collected using a contact time of 1 ms and a recycle delay of 5 s. ^1H spin-locking and decoupling frequencies of 38.5 and 19 kHz, respectively, were used. Approximately 120 free inductions decays were collected and averaged to obtain each ^{13}C spectrum. The ^{13}C chemical shifts were externally referenced to tetramethylsilane.

The ^{19}F and ^{31}P NMR spectra were measured with a single $\pi/2$ pulse (7.0 μs for ^{19}F and 6.7 μs for ^{31}P) and recycle delays of 20 s. A saturation-recovery pulse sequence was used to measure the spin-lattice relaxation of ^{19}F and ^{31}P nuclides. A comb of sixteen $\pi/2$ rf pulses were used to saturate the magnetization. Free induction decays were recorded after a $\pi/2$ observation pulse at varying delay times ranging from 0.1 to 25 seconds after saturation. Approximately 4 to 8 free inductions decays were averaged to obtain each ^{19}F and ^{31}P NMR spectrum. ^{19}F and ^{31}P chemical shifts were externally referenced to $CFCl_3$ and an aqueous solution of 85% H_3PO_4. The sample temperature in all experiments was controlled using hot or cold N_2 gas. The temperature calibration was performed using the well-known temperature dependence of the ^{207}Pb chemical shift of $Pb(NO_3)_2$.[37,38]

III. RESULTS AND DISCUSSION

A. Cation dynamics

The evolution of the ^{13}C static NMR spectra over the temperature range of 292 K to 174 K is shown in Fig. 2. The high-temperature ^{13}C NMR spectra of the liquid show the presence of eight distinct carbon sites 3 Me, Im 2, Im 4, Im 5, Bu 1, Bu 2, Bu 3, and Bu 4 characteristic of the $[C_4mim]^+$ cation with isotropic chemical shifts of 34.7, 135.4, 122.5, 121.2, 48.5, 30.6, 18.1, and 11.8 ppm, respectively. These spectra show slight broadening with decreasing temperature at temperatures above 246 K while a rapid broadening is observed upon at temperatures between 242 K and 218 K. No significant change in the ^{13}C NMR line shape is observed at temperatures

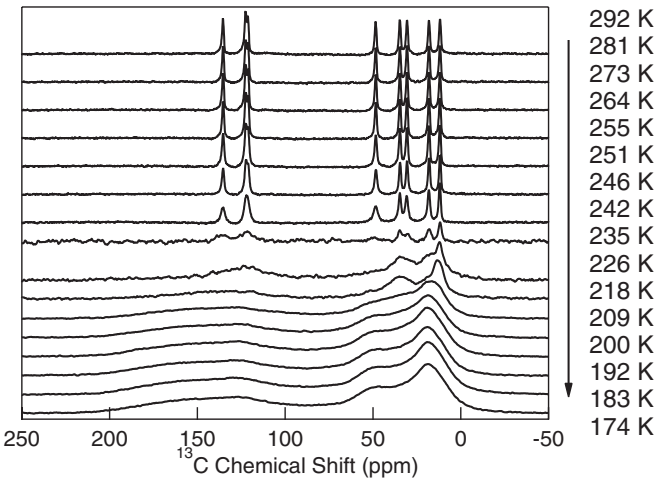

FIG. 2. Temperature dependence of the ^{13}C NMR spectra of $[C_4mim]PF_6$. The data were collected upon cooling.

below 209 K. The contribution of magnetic dipole-dipole interactions from ^1H nuclides towards spectral broadening is negligible due to HPPD. Therefore, the observed broadening of the ^{13}C NMR line shapes upon cooling in Fig. 2 results from an increasingly incomplete averaging of the ^{13}C chemical shift anisotropy (CSA) interaction indicating a slowing down of the reorientational motion of the cation.

The ^{13}C static NMR spectral line shapes have been simulated using a model of isotropic rotational reorientation (or tumbling) of the ^{13}C chemical shift tensors for each of the carbon sites in order to derive the characteristic timescale τ_{cation} of the reorientational dynamics of the cations. In this model, for each of the carbons sites the averaging of the CSA results from a random "exchange" among N different orientations under the rigid cation ($T \leqslant 209$ K) powder pattern. The orientational averaging of the ^{13}C CSA tensor was calculated separately for each of the carbon sites, and the resulting line shapes were added in order to produce the total simulated lineshape. The analytic expression for the resulting line shape for each CSA tensor is given by the real part of $g(\omega)$ where

$$g(\omega) = \frac{L}{N\left(1 - \frac{L}{\tau_{\text{cation}}}\right)} \tag{1}$$

$$L = \sum\nolimits_{j=1,N}\left[i(\omega - \omega_j) + \frac{1}{T_{2j}} + \frac{N}{\tau_{\text{cation}}}\right]^{-1}, \tag{2}$$

and ω_j is the frequency and T_{2j} is the reciprocal of the intrinsic linewidth corresponding to the orientation j.[39] In this analysis the frequencies j corresponding to 2000 or 4000 orientations (N) were generated by taking that many angular steps through the expression for the CSA powder pattern of each carbon site. The value of T_{2j} was set to be 2 ms to fit the ^{13}C NMR line shape at 292 K, which was considered to represent the extreme narrowing condition. It is to be noted that although the isotropic chemical shift δ_{iso} value for each of the carbon sites in the cation can be obtained from the ^{13}C NMR spectrum at 292 K, the principal components of chemical shift tensor δ_{11}, δ_{22}, and δ_{33} are required for the simulation and are not known *a priori* for these carbon sites in the cation. An experimental estimation of these quantities for the various

TABLE I. Isotropic chemical shift δ_{iso}, chemical shift anisotropy (CSA), and asymmetry parameter η of various carbon sites in the $[C_4mim]^+$ cation. CSA and η were calculated using DFT codes Gaussian 03 and CASTEP, while δ_{iso} was obtained from the experimental ^{13}C NMR spectrum of the RTIL above its melting point.

		CSA (ppm)		η	
Carbon site	δ_{iso} (ppm)	Gaussian 03	CASTEP	Gaussian 03	CASTEP
Im 2	135.4	93.9	114	0.8	0.37
Im 4	122.5	116.3	132.2	0.88	0.9
Im 5	121.2	119.4	126.9	0.86	0.92
Bu 1	48.5	47.3	61.5	0.91	0.8
3 Me	34.7	63.7	77.5	0.06	0.16
Bu 2	30.6	23.3	31.5	0.56	0.75
Bu 3	18.1	−21.7	−25.2	0.27	0.18
Bu 4	11.8	26.3	24.1	0.19	0.39

carbon sites is possible, in theory, from the corresponding ^{13}C NMR spectra of motionally rigid cation. However, the presence of multiple carbon sites in the $[C_4mim]^+$ cation results in strong signal overlap that makes such experimental estimation practically impossible from the one-dimensional, low-temperature rigid ion ^{13}C static spectrum (Fig. 2). These CSA tensor parameters for the different carbon sites were therefore calculated using *ab initio* density functional theory (DFT) based codes Gaussian 03 and CASTEP. All Gaussian 03[40] calculations for $[C_4mim]^+$ and PF_6^- were performed for the gas phase using 6-311+G(d,p) basis sets according to Becke's three-parameter hybrid method[41] with the LYP correlation functional (B3LYP).[42,43] All optimized structures were found to produce no imaginary frequencies, which ensured the presence of an energy minimum. The optimized cation structure with the *gauche*-transconformation of the butyl group[35] was adopted for the Gaussian 03 calculation. The corresponding ^{13}C NMR parameters were computed using the CSGT method.[44–46]

The DFT based codes CASTEP and CASTEP-NMR (Accelrys, Inc.) were used for calculations of the ^{13}C NMR parameters for the carbon sites in the $[C_4mim]PF_6$ crystal structure reported previously in the literature[47] without further geometry optimization.[48–51] The GIPAW algorithm and the generalized gradient approximation (GGA) simplified by Perdew-Burke-Ernzerhof (PBE) functional were employed.[48–51] An energy cutoff of 600 eV was used for the plane wave basis expansions. The Brillouin zone was sampled using the Monkhorst-Pack scheme and a $3 \times 3 \times 3$ k-point grid.[51] All core-valence interactions were modeled with ultrasoft pseudopotentials. These calculations yield the absolute shielding tensor principal components σ_{xx}, σ_{yy}, and σ_{zz}. The isotropic chemical shift δ_{iso} was obtained from isotropic shielding $\sigma_{iso} = 1/3(\sigma_{xx} + \sigma_{yy} + \sigma_{zz})$ using the relationship $\delta_{iso} = -(\sigma_{iso} - \sigma_{ref})$, where σ_{ref} is the isotropic shielding of a reference material. The carbon site in calcite ($CaCO_3$) crystal was used as a reference in this study, and its δ_{iso} was equated to the experimentally determined value of $\delta_{iso} = 168$ ppm. The ^{13}C CSA tensor parameters for the eight distinct carbon sites in the $[C_4mim]^+$ cation as obtained from Gaussian 03 and CASTEP calculations are summarized in Table I. These parameters are expressed in the form of anisotropy Δ and asymmetry parameter η, where $\Delta = 3(\sigma_{zz} - \sigma_{iso})/2$ and $\eta = (\sigma_{yy} - \sigma_{xx})/(\sigma_{zz} - \sigma_{iso})$ and their relative trends compare well between the two sets of calculations. These CSA parameters were subsequently used to calculate the rigid cation ^{13}C NMR spectrum of $[C_4mim]PF_6$. These calculated spectra, when compared against the experimental ^{13}C NMR spectrum of the $[C_4mim]PF_6$ glass collected in this study at 174 K, indicate that the ^{13}C NMR parameters obtained using the Gaussian 03 calculations yield somewhat better agreement with experiment compared with those obtained using CASTEP (Fig. 3). Therefore, these CSA parameters were subsequently used in the isotropic rotational reorientation model outlined previously to simulate the higher temperature ^{13}C NMR line shapes in order to obtain the τ_{cation} values for the different carbon sites in the $[C_4mim]^+$ cation. These simulated ^{13}C NMR line shapes are shown in Fig. 4 and are shown to compare well with the corresponding experimental line shapes over the entire range of temperatures explored in this study. All τ_{cation} values obtained from these line shape simulations are listed in Table II.

Figure 5 shows the τ_{cation} values for the various carbon sites plotted as a function of temperature. Clearly these τ_{cation} values are not uniform and can be broadly divided into two different groups, i.e., two different timescales of rotational motions of the cation. The τ_{cation} of the carbons in the imidazolium ring and the methyl groups (Im 2, Im 4, Im 5, 3 Me, and Bu 4) are smaller, i.e., they perform a faster isotropic rotational reorientation compared to the carbon atoms in the butyl group (Bu 1, Bu 2, Bu 3). This result is somewhat counterintuitive since the motion of the imidazolium ring is expected to be influenced by the strong coulombic interaction; hence, its rotational motion should be slower than that of the butyl group. Previous ^1H and ^{13}C NMR T_1 results of RTILs demonstrated, in line with this expectation, that the rotational motion of the ring responsible for spin-lattice relaxation was indeed slower than that of the alkyl groups.[52–61]

This apparent discrepancy between the ^{13}C NMR results obtained in this study and previous ^1H and ^{13}C NMR T_1 measurements can be explained as follows: RTILs with long alkyl chains such as $[C_4mim]PF_6$ are considered to possess local structures (or nanostructure) in the form of polar and nonpolar domains in the liquid state.[62–67] The existence of this local structure will inhibit reorientational motions accompanied with exchange of a charged ring and a nonpolar butyl group position. In fact, it is known that the rotational motions

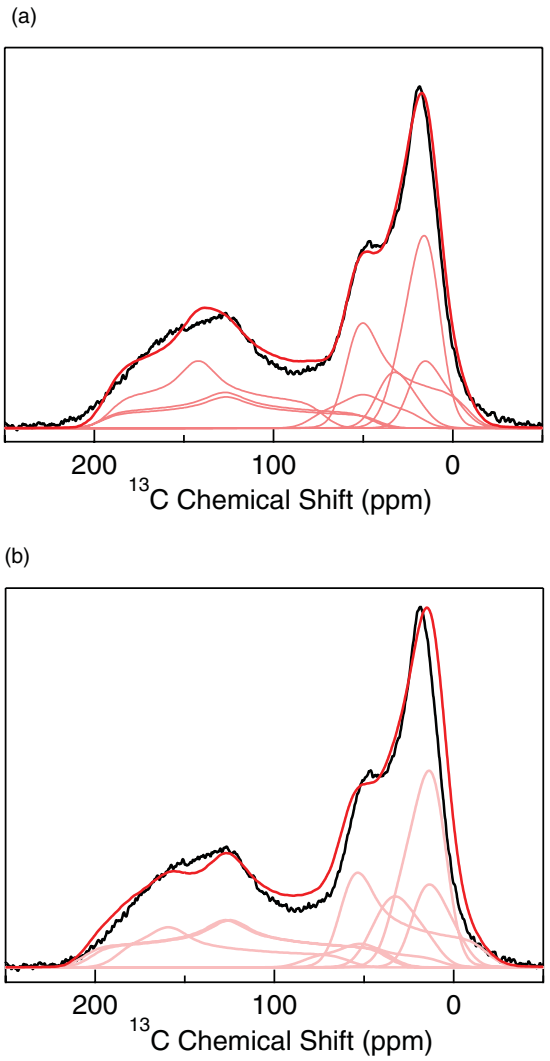

FIG. 3. (Color online) Experimental (black) and simulated (red/gray) ^{13}C NMR spectra at 174 K with (a) Gaussian 03 (b) CASTEP. Total simulated spectra and the individual simulation components are shown as thick and thin red (gray) lines, respectively.

of some imidazolium-based RTILs are anisotropic.[61,68–70] In addition, and perhaps more importantly, the isotropic rotation of the butyl group would be accompanied by a large change in the cation shape that could also be restricted by the existence of the local structure. The previous T_1 results indicated a slower dynamics of the imidazolium ring compared to that the alkyl chain possibly because the NMR spin-lattice relaxation in these liquids probe small-angle rotations and/or librational motions of the ions (see section on anion dynamics below).[57,59] Such motions would have significantly smaller activation energy barriers compared to that experienced by the rotational reorientation probed here using ^{13}C NMR line shape analyses. Therefore, our findings clearly suggest that the rotational isomerization of the butyl group is slower than the isotropic reorientation of the imidazolium ring in the supercooled region.

B. Anion dynamics

Figure 6 shows the NMR spectra of the ^{19}F and ^{31}P nuclides in the PF_6^- anions. The ^{19}F and ^{31}P NMR spectra of the

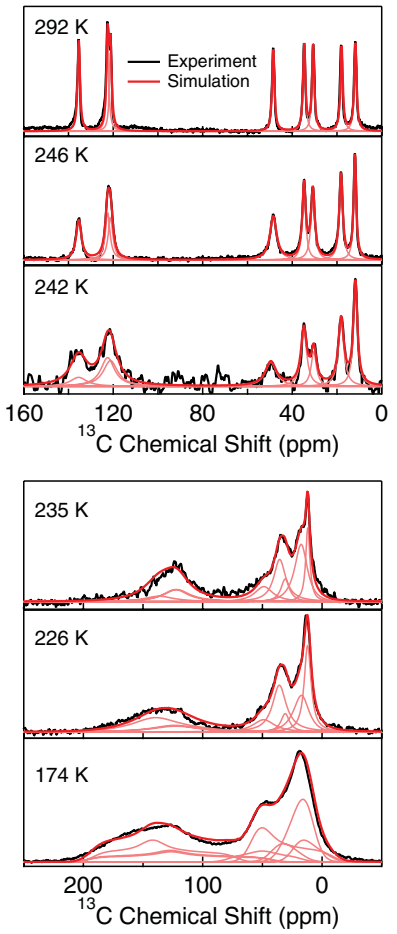

FIG. 4. (Color online) Experimental (black) and simulated (red/gray) ^{13}C NMR spectra at 292 K, 246 K, 242 K, 235 K, 226 K, and 174 K. Simulated spectra are based on the ^{13}C NMR CSA parameters for the rigid lattice calculated using Gaussian 03. Total simulated spectra and the individual simulation components are shown as thick and thin red (gray) lines, respectively.

liquid show the presence of one F and one P site where the corresponding signal is split by the ^{19}F $\leftrightarrow$ ^{31}P J coupling into two and seven peaks, respectively. The corresponding isotropic ^{19}F and ^{31}P chemical shifts are -73.6 and -143.6 ppm, respectively, and the magnitude of the J_{P-F} coupling is $\sim$710 Hz. Both ^{19}F and ^{31}P spectra start to broaden with decreasing temperature below 235 K. The line broadening in these spectra is mainly governed by the magnetic dipole-dipole

TABLE II. Rotational relaxation times τ_{cation} (μs) of the CSA tensors of various carbon sites in the $[C_4mim]^+$ cation.

Carbon site	246 K	242 K	235 K	226 K
Im 2	1	5	20	50
Im 4	0.5	2.5	10	20
Im 5	0.5	2.5	10	20
Bu 1	5	10	40	50
3 Me	1	3.3	17	20
Bu 2	5	17	50	50
Bu 3	5	14	110	170
Bu 4	1	6.7	17	33

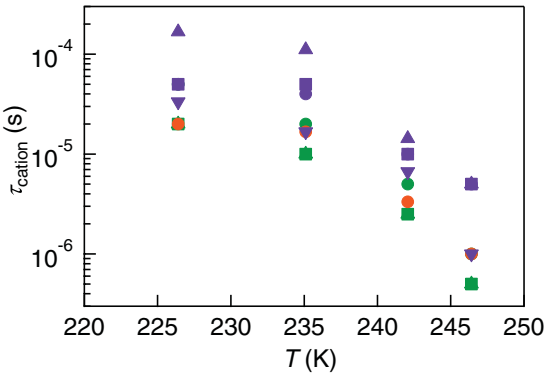

FIG. 5. (Color online) Characteristic timescale τ_{cation} of rotational reorientation of the ^{13}C chemical shift tensor for each of the carbon sites in the cation. Green (gray) symbols represent carbon sites in the imidazolium ring: Im 2 (circles), Im 4 (squares), and Im 5 (triangles). Purple (medium gray) symbols represent carbon sites in the butyl group: Bu 1 (circles), Bu 2 (squares), Bu 3 (triangles), and Bu 4 (inverted triangles). Orange (light gray) circles represent 3 Me carbons.

interactions. In the case of the ^{31}P nuclides the magnetic dipole-dipole interaction is dominated by the heteronuclear $^{31}P \leftrightarrow {}^{19}F$ dipolar coupling from the six nearest-neighbor ^{19}F nuclides in the PF_6^- anions. A relatively minor but non-negligible source of dipolar-line broadening in the ^{31}P NMR spectra may be associated with $^{31}P \leftrightarrow {}^{1}H$ dipolar coupling from the protons in the neighboring cations. On the other hand, there are multiple important contributions to the dipolar broadening for ^{19}F nuclides including the homonuclear $^{19}F \leftrightarrow {}^{19}F$ dipolar coupling between intra- and intermolecular ^{19}F, heteronuclear $^{19}F \leftrightarrow {}^{31}P$ dipolar coupling from P-F bonds in the anion, and $^{19}F \leftrightarrow {}^{1}H$ dipolar coupling from the protons in the neighboring cations. Thus, the broadening of the ^{19}F and ^{31}P NMR line shapes at temperatures below 235 K must be indicative of incomplete averaging of the aforementioned dipolar interactions due to the slowing down of the ionic dynamics. It should be noted here that this broadening of the ^{19}F and ^{31}P NMR line shapes is found to be completely reversible upon reheating to temperatures above 235 K subsequent to cooling down of the sample to 174 K and

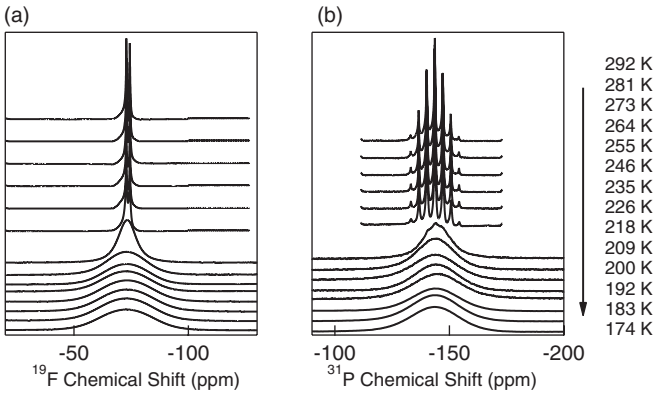

FIG. 6. Temperature dependence of the (a) ^{19}F and (b) ^{31}P NMR spectra of $[C_4mim]PF_6$. The data were collected upon cooling.

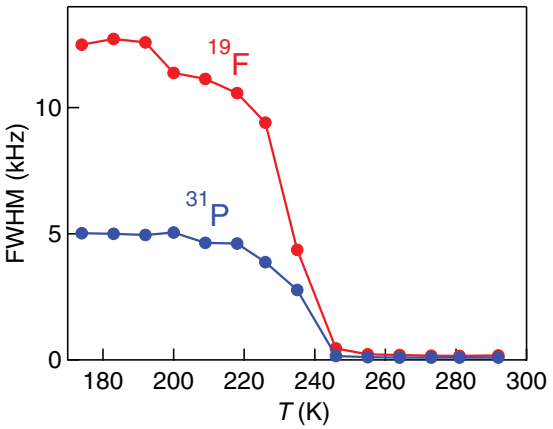

FIG. 7. (Color online) Temperature dependence of the full width at half-maximum (FWHM) of ^{19}F (red circles) and ^{31}P (blue circles) spectra.

therefore does not correspond to any possible crystallization of the sample.

The temperature dependence of the full width at half-maximum (FWHM) of the ^{19}F and ^{31}P spectra are found to be similar and are shown in Fig. 7. The FWHM of the ^{19}F and ^{31}P NMR line shapes increases rapidly with decreasing temperature in the range of 246 K to 218 K and becomes almost constant below 218 K. The rapid increase of the ^{19}F and ^{31}P FWHM over a narrow temperature range may correspond to the onset of a caging effect on the ionic dynamics upon cooling, and this temperature range seems to be more closely related to the crystallization temperature (227 K)[35] of the $[C_4mim]PF_6$ liquid rather than its glass transition temperature T_g (192 K). However, in the absence of any crystallization event in the sample it is tempting to relate this onset temperature for caging of the ionic dynamics to the mode-coupling transition temperature T_c that signifies a dynamical transition from free Brownian diffusion to thermally activated motion in a liquid. The critical temperature T_c in the mode coupling theory of glass transitions[8] can be obtained from the high-temperature viscosity of a liquid using the following expression:

$$\eta(T) \propto (T - T_C)^{-\gamma}, \tag{3}$$

where η is the viscosity, T is the temperature, and γ is the power-law exponent that typically varies between 2 and 4. The T_c value obtained from the viscosity data of the $[C_4mim]PF_6$ liquid[71] is ~232 K that is indeed in good agreement with the temperature where the FWHM of the ^{19}F and ^{31}P NMR line shapes show an abrupt increase upon cooling (Fig. 7).

The maximum FWHM values of the ^{19}F and ^{31}P NMR spectra around T_g are estimated to be ~13 kHz and 5 kHz, respectively. For a rigid lattice NMR line shape with Gaussian dipolar broadening, the FWHM can be expressed in the form of its second moment M_2 as[72]

$$FWHM = 2.35\sqrt{M_2} \tag{4}$$

$$M_2(\text{Gauss}^2) = \frac{3}{5}\gamma_I^2\hbar^2 N^{-1} I(I+1)\sum_{j,k} r_{jk}^{-6} + \frac{4}{15}\gamma_S^2\hbar^2 N^{-1} S(S+1)\sum_{j,f} r_{jf}^{-6}, \tag{5}$$

where γ is the gyromagnetic ratio, $\hbar$ is the reduced Planck's constant, N is the number of nuclei, I and S are the nuclear spin quantum numbers for the resonant and nonresonant spins, respectively, and r is the distance between spin pairs j and f, or j and k. The approximate FWHM values of ^{19}F and ^{31}P spectra in a rigid "lattice" of glassy $[C_4mim]PF_6$ can then be estimated from Eqs. (4) and (5) using the r values from the crystal structure.[47] Such estimates yield the FWHM of the ^{19}F and ^{31}P NMR line shapes to be 36.4 kHz and 29.5 kHz, respectively. The observed FWHM values around T_g are thus much smaller than the estimated ones, implying dynamical averaging of the corresponding dipolar interaction. Moreover, the fact that the full dipolar FWHM is not recovered even around T_g is indicative of partial averaging of the ^{19}F and ^{31}P dipolar coupling interactions even in the glassy state. This partial averaging may result from a restricted rotational motion of the PF_6^- anions that onsets around and below 230 K. However, it is important to note that the respective residual ^{19}F and ^{31}P FWHM values of ~13 and 5 KHz around T_g are remarkably close to that expected from ^{19}F $\leftrightarrow$ ^{1}H and ^{31}P $\leftrightarrow$ ^{1}H rigid lattice-dipolar couplings (16 and 5 kHz, respectively) from the protons in the neighboring cations. Therefore, perhaps a more plausible dynamical scenario is that the rapid rotational reorientation of the PF_6^- anions continues over the entire temperature range that averages out the strong ^{19}F $\leftrightarrow$ ^{19}F and ^{31}P $\leftrightarrow$ ^{19}F dipolar couplings. The ^{19}F and ^{31}P FWHM values around and below 230 K are then controlled by the dynamical slowdown of the $[C_4mim]^+$ cations that results in progressive freezing of the orientational averaging of ^{19}F $\leftrightarrow$ ^{1}H and ^{31}P $\leftrightarrow$ ^{1}H dipolar interactions. This hypothesis is consistent with the general similarity in the temperature dependences of the τ_{cation} and the ^{19}F and ^{31}P FWHM values below ~250 K (Figs. 5 and 7) and the fact that below 230 K the τ_{cation} becomes long enough ($\sim 10^{-4}$ s) to lead to incomplete averaging of the ^{19}F $\leftrightarrow$ ^{1}H and ^{31}P $\leftrightarrow$ ^{1}H dipolar interactions. When taken together, these results imply that around and below 230 K the isotropic rotational reorientation of the PF_6^- anion decouples from that of the $[C_4mim]^+$ cations responsible for the α relaxation.

Figure 8 shows the temperature dependence of T_1 for both ^{19}F and ^{31}P nuclides. The T_1 for both nuclides shows similar variation with temperature, much like the similarity in the variation of the FWHM of the ^{19}F and ^{31}P NMR line shapes, as shown in Fig. 7. Although no T_1 minimum is observed within the temperature range studied here, the shape of these T_1 vs T curves suggests the presence of possibly two T_1 minima, one near 180 K and the other at temperatures above 280 K. Since the characteristic correlation timescale of the motion responsible for spin-lattice relaxation $\tau \sim 1/\omega$, where ω is the resonance frequency of the ^{19}F or ^{31}P nuclide, τ is expected to be on the order of nanoseconds at temperatures near the T_1 minima. Since one of these T_1 minima is below T_g, these results again indicate substantial motion of the PF_6^- anions even in the glassy state, perhaps in the form of a librational or restricted rotational motion at the nanosecond timescale. In this dynamical scenario the second T_1 minimum above 280 K would correspond to an isotropic rotational reorientation of the PF_6^- anions at nanosecond timescale that is presumably coupled to viscous flow and shear relaxation of the liquid (*vide infra*).

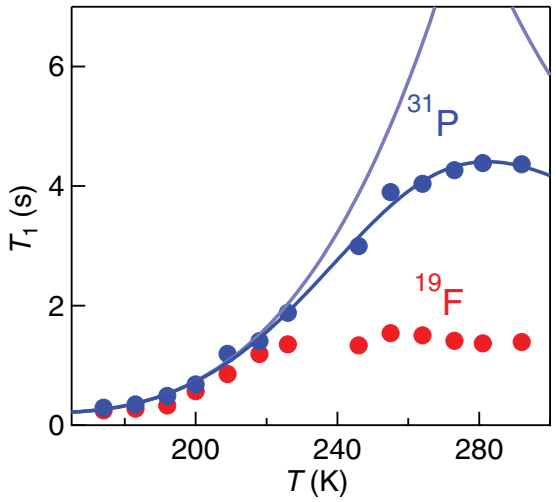

FIG. 8. (Color online) Temperature dependence of ^{19}F (red) and ^{31}P (blue) T_1. Simulation of the ^{31}P T_1 data is shown as dark blue line, and the individual simulation components for the low and high temperature dynamical components are shown as light blue lines. See text for details of the simulation.

Quantitative modeling of these spin-lattice relaxation results may allow us to obtain further information regarding the dynamics of the PF_6^- anions. There are five possible contributions to the nuclear spin-lattice relaxation mechanism that can be expressed as follows:

$$\frac{1}{T_1} = \frac{1}{T_1^{DD}} + \frac{1}{T_1^{CSA}} + \frac{1}{T_1^{SR}} + \frac{1}{T_1^{Sc}} + \frac{1}{T_1^{Q}}, \tag{6}$$

where $T_1{}^{DD}$, $T_1{}^{CSA}$, $T_1{}^{SR}$, $T_1{}^{Sc}$, and $T_1{}^{Q}$ are the relaxation times associated with magnetic dipole-dipole, CSA, spin rotation, scalar, and quadrupole interactions, respectively. The relaxation mechanisms of both ^{19}F and ^{31}P nuclei should be dominated by the magnetic dipole-dipole interactions, i.e.,

$$\frac{1}{T_1} \approx \frac{1}{T_1^{DD}}. \tag{7}$$

The main dipolar interaction for the ^{19}F nuclei is homonuclear in nature while that for ^{31}P is heteronuclear between ^{31}P and ^{19}F nuclides within the PF_6^- anions. The resulting $T_1{}^{DD}$ for ^{19}F nuclides can be written as[73,74]

$$\frac{1}{T_1^{DD}} = \frac{3N_F}{20}(2\pi D_{FF})^2[J(\omega_F) + 4J(2\omega_F)] \tag{8}$$

and that for ^{31}P nuclides can be written as[73,74]

$$\frac{1}{T_1^{DD}} = \frac{N_F}{20}(2\pi D_{PF})^2[J(\omega_P - \omega_F) + 3J(\omega_P) + 6J(\omega_P + \omega_F)] \tag{9}$$

$$D = \frac{\mu_0}{4\pi}\frac{\hbar}{2\pi}\frac{\gamma^2}{r^3} \tag{10}$$

$$J(\omega) = \frac{2\tau_{anion}}{1 + (\omega\tau_{anion})^2} \tag{11}$$

$$\tau_{anion} = \tau_0 \exp\left(\frac{E_a}{RT}\right), \tag{12}$$

TABLE III. Dipolar coupling constants D, correlation time at infinite temperature τ_0, and activation energy E_a obtained from simulation of the ^{31}P T_1 data (see text for details).

	D (kHz)	τ_0 (s)	E_a (eV)
^{31}P fast	10.3	7×10^{-15}	0.16
^{31}P slow	10.3	3×10^{-10}	0.12

where D is the dipolar coupling constant, $J(\omega)$ is the spectral density, μ_0 is the permeability of vacuum, τ_{anion} is the rotational correlation time of PF_6^-, τ_0 is the correlation time at infinite temperature, E_a is the activation energy for rotational dynamics, and R is the gas constant. The r values are the internuclear ^{19}F – ^{19}F and ^{31}P – ^{19}F distances in the PF_6^- anion. The D value for ^{31}P nuclei was calculated using structural parameters from Gaussian 03 simulations to be ~10.3 kHz and was kept fixed in the fit. The D value for ^{19}F could not be fixed due to the presence of aforementioned multiple contributions to the dipolar coupling to ^{19}F T_1^{DD}. As a result only the ^{31}P T_1 data are fitted with Eq. (9) as two separate dynamical processes, namely, an isotropic rotational reorientation that dominates at high temperatures and a librational or restricted rotational motion that is dominant at lower temperatures, as discussed previously. The parameters for the low-temperature librational motion as obtained from fitting the T_1 measurements are listed in Table III, and the correlation times τ_{anion} are shown in Fig. 9 as a function of temperature. We do not discuss the high-temperature isotropic rotational motion since there are not enough T_1 data to obtain reliable parameters for this process. The τ_{anion} values obtained from fitting the low-temperature ^{31}P T_1 data correspond to the librational motion of the rigid anion PF_6^-. The activation energy of this motion is found to be ~0.16 eV (Table III).

C. Comparison of relaxation times to previous results

As mentioned previously, $[C_4mim]PF_6$ is one of the most well studied ionic liquids in relation to the glass transition phenomena in RTILs. The previously reported relaxation times

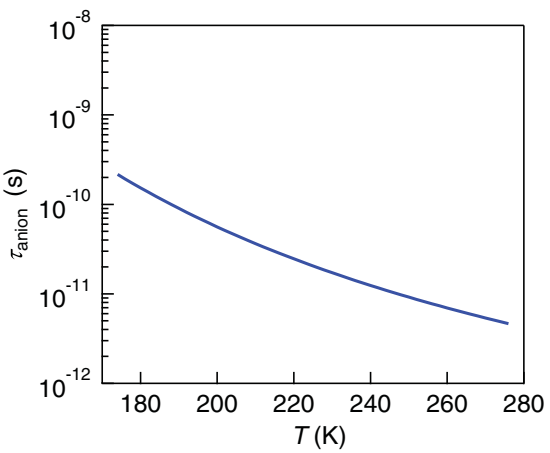

FIG. 9. (Color online) Temperature dependence of rotational correlation times τ_{anion} of PF_6^- anions obtained from simulation of the ^{31}P T_1 data in Fig. 8.

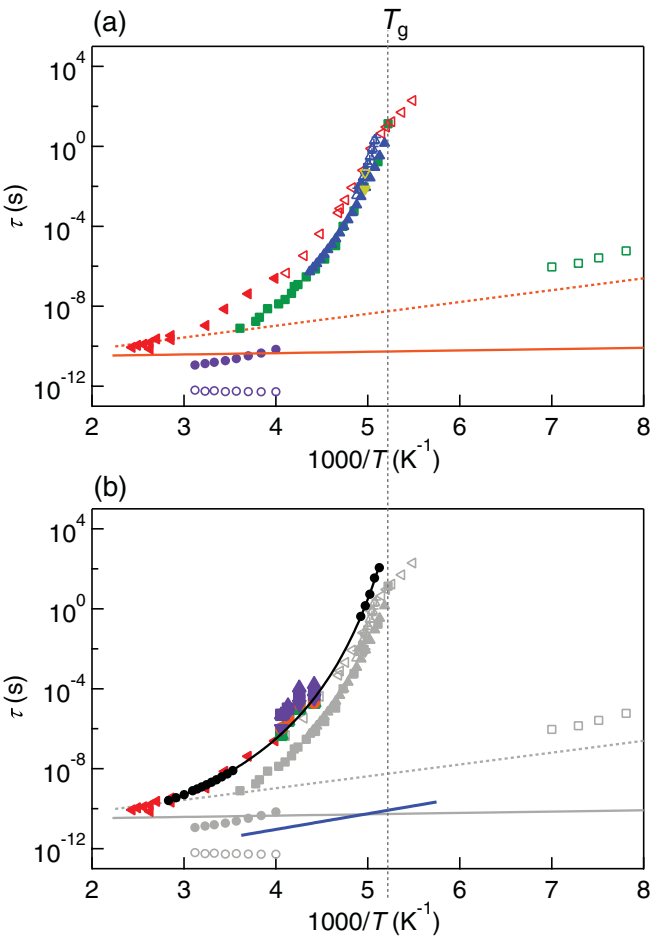

FIG. 10. (Color online) (a) The previously reported relaxation times in the $[C_4mim]PF_6$ system as determined by dielectric spectroscopy (■, □, and ◁),[18,19] depolarized light-scattering (◀),[19] thermal relaxation (▼ and ▽),[23] solvation dynamics (▲, △, and +),[32] and quasielastic neutron scattering (● and ○, and orange solid and dashed lines).[28,30] (b) The reported relaxation times shown in Fig. 10(a) (gray), τ_{vis} estimated from the viscosity data[34,71] when $G_\infty = 10^8$ Pa and the VFT fit (black), relaxation times τ_{DLS} from depolarized light-scattering study by Rivera *et al.*[19] (◀), and the relaxation times τ_{cation} (green, purple, and orange symbols, see Fig. 5 for explanation) and τ_{anion} (blue line) obtained in this study.

in the $[C_4mim]PF_6$ system as determined by a wide range of spectroscopic and scattering techniques including dielectric spectroscopy, depolarized light scattering, thermal relaxation, solvation dynamics, and quasielastic neutron scattering are summarized in Fig. 10(a).[18,19,23,28,30,32] Though for the detailed discussion of these results the reader should be referred to the original papers, here we mention two important features of the relaxation processes in this RTIL: (1) both α- and β-relaxation processes have been observed in $[C_4mim]PF_6$, and (2) the timescale of the translational motion of the ions becomes decoupled from that of the rotational motion close to T_g. These two features are the hallmarks of the dynamics of glass-forming liquids. However, direct observation of the atomic scale motions of cations and anions and linking their relative contributions to these relaxation processes have remained somewhat speculative.

Figure 10(b) displays a comparison between the temperature dependence of the τ_{cation} as determined in this study, the structural relaxation time measured by Rivera *et al.*[19] with depolarized light scattering in this RTIL and its shear relaxation time τ_{vis} obtained from the viscosity data[34,70] using the Maxwell relation $\tau_{vis} = \frac{\eta}{G_\infty}$, where G_∞ is the instantaneous shear modulus taken to be 10^8 Pa and independent of temperature and η is the viscosity. It is clear that these three timescales are in excellent agreement and structural/α relaxation in this ionic liquid is controlled by the isotropic rotational reorientation of the constituent cations that is faithfully probed by dynamical averaging of the ^{13}C CSA interactions and by depolarized light scattering.

On the other hand, the temperature dependence of the τ_{anion} values determined in this study is found to be similar to those of the β-relaxation times obtained in previous studies using dielectric spectroscopy and quasielastic neutron scattering.[18,30] Therefore, the librational motion of the PF_6^- anions can be attributed to the β-relaxation process. It is to be noted that a number of previous studies attributed the microscopic origin of β relaxations in RTILs to hydrogen dynamics in the alkyl groups of cations.[16,18,30,75,76] The results presented in this study do not contradict that scenario but indicate that anionic motions in RTILs can also contribute to the β-relaxation process. However, a mechanistic understanding of the temporal coupling between the cationic and anionic motions associated with the β relaxation remains lacking at this stage.

IV. SUMMARY

The dynamics of the cations and the anions in the RTIL $[C_4mim]PF_6$ has been studied using multinuclear NMR spectroscopy. ^{13}C NMR line-shape analyses reveal that the average timescale of the rotational reorientation of the cations τ_{cation} corresponds well with that of the primary or α relaxation in the supercooled liquid state. The timescale of motional averaging of the ^{13}C CSA interactions for carbon sites in the imidazolium ring and in the two methyl groups (Im 2, Im 4, Im 5, 3 Me, and Bu 4) are found to be faster than that of the three carbon atoms in the butyl chain (Bu 2, Bu 3, and Bu 4). Therefore, the butyl chain reorientational motions, which are reminiscent of the conformational isomerization, are slower than the imidazolium ring reorientation.

FWHM analyses of the ^{19}F and ^{31}P spectra indicate that the rotational dynamics of the PF_6^- anions continues well into the glassy state and temporally decouples from the dynamics of the $[C_4mim]^+$ cations responsible for the α relaxation around the mode-coupling critical temperature T_c ($\sim$230 K) possibly implying the onset of a caging effect. The ^{19}F and ^{31}P T_1 data are consistent with this dynamical scenario and indicate that the anionic dynamics is dominated by isotropic rotational diffusion at temperatures $T > T_c$ and by librational motion below T_c. The rotational diffusion of the anion is possibly coupled to the α relaxation above T_c, while the librational timescale τ_{anion} (10^{-10} s) and its activation energy (0.16 eV) are characteristic of a β-relaxation process.

ACKNOWLEDGMENTS

The present study was supported by the Ministry of Education, Culture, Sports, Science and Technology of Japan No. 21245003 Grant-in-Aid for Scientific Research (A) and the Global Center-of-Excellence Program "Advanced School for Organic Electronics." This work was also supported by Japan Society for the Promotion of Science "Frontier science international training program for young researchers leading in materials science and computational science." S.S. was supported by NSF Grant DMR-0906070.

*To whom correspondence should be addressed: sbsen@ucdavis.edu.

[1] P. Wasserscheid and T. Welton, *Ionic Liquids in Synthesis* (VCH-Wiley, Weinheim, Germany, 2003).
[2] H. Ohno, *Electrochemical Aspects of Ionic Liquids* (Wiley-Interscience, Hoboken, 2005).
[3] T. Welton, Chem. Rev. **99**, 2071 (1999).
[4] P. Wasserscheid and W. Keim, Angew. Chem. Int. Ed. **39**, 3772 (2000).
[5] R. Sheldon, Chem. Commun. 2399 (2001).
[6] H. Sillescu, J. Non-Cryst. Solids **243**, 81 (1999).
[7] P. G. Debenedetti and F. H. Stillinger, Nature **410**, 259 (2001).
[8] S. P. Das, Rev. Mod. Phys. **76**, 785 (2004).
[9] G. Tarjus, S. A. Kivelson, Z. Nussinov, and P. Viot, J. Phys. Condens. Matter **17**, R1143 (2005).
[10] J. J. Moura Ramos, C. A. M. Afonso, and L. C. Branco, J. Therm. Anal. Cal. **71**, 659 (2003).
[11] G. J. Kabo, A. V. Blokhin, Y. U. Paulechka, A. G. Kabo, M. P. Shymanovich, and J. W. Magee, J. Chem. Eng. Data **49**, 453 (2004).
[12] H. P. Diogo and J. J. M. Ramos, Phase Transit. **78**, 357 (2005).
[13] O. Yamamuro, Y. Inamura, S. Hayashi, and H. Hamaguchi, AIP Conf. Proc. **832**, 73 (2006).
[14] O. Yamamuro, Y. Minamimoto, Y. Inamura, S. Hayashi, and H. Hamaguchi, Chem. Phys. Lett. **423**, 371 (2006).
[15] Y. Shimizu, Y. Ohte, Y. Yamamura, K. Saito, and T. Atake, J. Phys. Chem. B **110**, 13970 (2006).
[16] A. Triolo, A. Mandanici, O. Russina, V. Rodriguez-Mora, M. Cutroni, C. Hardacre, M. Nieuwenhuyzen, H.-J. Bleif, L. Keller, and M. A. Ramos, J. Phys. Chem. B **110**, 21357 (2006).
[17] N. Ito, W. Huang, and R. Richert, J. Phys. Chem. B **110**, 4371 (2006).
[18] A. Rivera and E. A. Rössler, Phys. Rev. B **73**, 212201 (2006).
[19] A. Rivera, A. Brodin, A. Pugachev, and E. A. Rössler, J. Chem. Phys. **126**, 114503 (2007).
[20] A. Rivera-Calzada, K. Kaminski, C. Leon, and M. Paluch, J. Phys. Chem. B **112**, 3110 (2008).
[21] J. Leys, M. Wübbenhorst, C. Preethy Menon, R. Rajesh, J. Thoen, C. Glorieux, P. Nockemann, B. Thijs, K. Binnemans, and S. Longuemart, J. Chem. Phys. **128**, 064509 (2008).

[22]J. R. Sangoro, C. Iacob, A. Serghei, C. Friedrich, and F. Kremer, Phys. Chem. Chem. Phys. **11**, 913 (2009).
[23]W. Huang and R. Richert, J. Chem. Phys. **131**, 184501 (2009).
[24]Z. Wojnarowska, M. Paluch, A. Grzybowski, K. Adrjanowicz, K. Grzybowska, K. Kaminski, P. Wlodarczyk, and J. Pionteck, J. Chem. Phys. **131**, 104505 (2009).
[25]Z. Wojnarowska, K. Grzybowska, A. Grzybowski, M. Paluch, K. Kaminski, P. Wlodarczyk, K. Adrjanowicz, and J. Pionteck, J. Chem. Phys. **132**, 094506 (2010).
[26]K. Nakamura, T. Saiwaki, and K. Fukao, Macromolecules **43**, 6092 (2010).
[27]J. R. Sangoro, C. Iacob, S. Naumov, R. Valiullin, H. Rexhausen, J. Hunger, R. Buchner, V. Strehmel, J. Kärger, and F. Kremer, Soft Matter **7**, 1678 (2011).
[28]A. Triolo, O. Russina, V. Arrighi, F. Juranyi, S. Janssen, and C. M. Gordon, J. Chem. Phys. **119**, 8549 (2003).
[29]W. Xu, E. I. Cooper, and C. A. Angell, J. Phys. Chem. B **107**, 6170 (2003).
[30]A. Triolo, O. Russina, C. Hardacre, M. Nieuwenhuyzen, M. A. Gonzalez, and H. Grimm, J. Phys. Chem. B **109**, 22061 (2005).
[31]M. C. C. Ribeiro, J. Phys. Chem. B **111**, 5008 (2007).
[32]N. Ito and R. Richert, J. Phys. Chem. B **111**, 5016 (2007).
[33]K. L. Ngai, J. Phys. Chem. B **110**, 26211 (2006).
[34]N. Shamim and G. B. McKenna, J. Phys. Chem. B **114**, 15742 (2010).
[35]T. Endo, T. Kato, K. Tozaki, and K. Nishikawa, J. Phys. Chem. B **114**, 407 (2010).
[36]A. E. Bennett, C. M. Rienstra, M. Auger, K. V. Lakshmi, and R. G. Griffin, J. Chem. Phys. **103**, 6951 (1995).
[37]A. Bielecki and D. P. Burum, J. Magn. Reson. A **116**, 215 (1995).
[38]T. Takahashi, H. Kawashima, H. Sugisawa, and T. Baba, Solid State Nucl. Magn. Reson. **15**, 119 (1999).
[39]M. Mehring, *Principles of High Resolution NMR in Solids* (Springer-Verlag, Berlin, 1983).
[40]M. J. Frisch *et al*., *Gaussian 03*, Wallingford, Connecticut, 2004.
[41]A. D. Becke, J. Chem. Phys. **98**, 5648 (1993).
[42]C. Lee, W. Yang, and R. G. Parr, Phys. Rev. B **37**, 785 (1988).
[43]B. Miehlich, A. Savin, H. Stoll, and H. Preuss, Chem. Phys. Lett. **157**, 200 (1989).
[44]T. A. Keith and R. F. W. Bader, Chem. Phys. Lett. **194**, 1 (1992).
[45]T. A. Keith and R. F. W. Bader, Chem. Phys. Lett. **210**, 223 (1993).
[46]J. R. Cheeseman, J. Chem. Phys. **104**, 5497 (1996).
[47]A. R. Choudhury, N. Winterton, A. Steiner, A. I. Cooper, and K. A. Johnson, J. Am. Chem. Soc. **127**, 16792 (2005).
[48]F. Mauri, B. G. Pfrommer, and S. G. Louie, Phys. Rev. Lett. **77**, 5300 (1996).
[49]J. P. Perdew, K. Burke, and M. Ernzerhof, Phys. Rev. Lett. **77**, 3865 (1996).
[50]C. J. Pickard and F. Mauri, Phys. Rev. B **63**, 245101 (2001).
[51]M. D. Segall, P. J. D. Lindan, M. J. Probert, C. J. Pickard, P. J. Hasnip, S. J. Clark, and M. C. Payne, J. Phys. Condens. Matter **14**, 2717 (2002).
[52]W. R. Carper, J. L. Pflug, A. M. Elias, and J. S. Wilkes, J. Phys. Chem. **96**, 3828 (1992).
[53]C. E. Keller and W. R. Carper, Inorg. Chim. Acta **238**, 115 (1995).
[54]J. H. Antony, D. Mertens, A. Dölle, P. Wasserscheid, and W. R. Carper, ChemPhysChem **4**, 588 (2003).
[55]W. R. Carper, P. G. Wahlbeck, J. H. Antony, D. Mertens, A. Dölle, and P. Wasserscheid, Anal. Bioanal. Chem. **378**, 1548 (2004).
[56]J. H. Antony, D. Mertens, T. Breitenstein, A. Dölle, P. Wasserscheid, and W. R. Carper, Pure Appl. Chem. **76**, 255 (2004).
[57]K. Hayamizu, S. Tsuzuki, and S. Seki, J. Phys. Chem. A **112**, 12027 (2008).
[58]M. Imanari, K. Uchida, K. Miyano, H. Seki, and K. Nishikawa, Phys. Chem. Chem. Phys. **12**, 2959 (2010).
[59]T. Endo, M. Imanari, H. Seki, and K. Nishikawa, J. Phys. Chem. A **115**, 2999 (2011).
[60]J. H. Antony, A. Dölle, D. Mertens, P. Wasserscheid, W. R. Carper, and P. G. Wahlbeck, J. Phys. Chem. A **109**, 6676 (2005).
[61]N. E. Heimer, J. S. Wilkes, P. G. Wahlbeck, and W. R. Carper, J. Phys. Chem. A **110**, 868 (2006).
[62]K. Iwata, H. Okajima, S. Saha, and H. Hamaguchi, Acc. Chem. Res. **40**, 1174 (2007).
[63]A. A. H. Pádua, M. F. Costa Gomes, and J. N. A. Canongia Lopes, Acc. Chem. Res. **40**, 1087 (2007).
[64]L. P. N. Rebelo, J. N. Canongia Lopes, J. M. S. S. Esperança, H. J. R. Guedes, J. Łachwa, V. Najdanovic-Visak, and Z. P. Visak, Acc. Chem. Res. **40**, 1114 (2007).
[65]H. Weingärtner, Angew. Chem. Int. Ed. **47**, 654 (2008).
[66]E. W. Castner and J. F. Wishart, J. Chem. Phys. **132**, 120901 (2010).
[67]A. Triolo, O. Russina, B. Fazio, R. Triolo, and E. Di Cola, Chem. Phys. Lett. **457**, 362 (2008).
[68]Y. Shim and H. J. Kim, J. Phys. Chem. B **112**, 11028 (2008).
[69]K. Nakamura and T. Shikata, ChemPhysChem **11**, 285 (2010).
[70]B. Qiao, C. Krekeler, R. Berger, L. D. Site, and C. Holm, J. Phys. Chem. B **112**, 1743 (2008).
[71]W. Fan, Q. Zhou, J. Sun, and S. Zhang, J. Chem. Eng. Data **54**, 2307 (2009).
[72]J. H. Van Vleck, Phys. Rev. **74**, 1168 (1948).
[73]N. Bloembergen, E. M. Purcell, and R. V. Pound, Phys. Rev. **73**, 679 (1948).
[74]A. Abragam, *Principles of Nuclear Magnetism* (Oxford University Press, Oxford, 1961).
[75]O. Russina, M. Beiner, C. Pappas, M. Russina, V. Arrighi, T. Unruh, C. L. Mullan, C. Hardacre, and A. Triolo, J. Phys. Chem. B **113**, 8469 (2009).
[76]O. Yamamuro, T. Yamada, M. Kofu, M. Nakakoshi, and M. Nagao, J. Chem. Phys. **135**, 054508 (2011).